The strength of El Niño and the spatial extent of tropical drought

Bradfield Lyon

International Research Institute for Climate Prediction, Lamont-Doherty Earth Observatory, Columbia University, New York, New York, USA

Received 1 July 2004; revised 16 September 2004; accepted 4 October 2004; published 6 November 2004.

[1] During El Niño events, several spatially coherent, nearly synchronous droughts typically develop in teleconnected tropical land areas. These droughts, reflected in below-average tropical mean land area precipitation, are frequently accompanied by multiple and wide ranging impacts. Here it is shown, based on precipitation observations for the past half-century, that there is a remarkably robust relationship between El Niño strength and the spatial extent of drought in the global tropics. Not reported previously, drought covers more than twice the land area in strong versus weak El Niños and in many areas severe drought is shown to be more likely during El Niño than for all other times. The results provide insight into large-scale tropical rainfall variability and have implications for future droughts under global warming scenarios. *INDEX TERMS:* 1812 Hydrology: Drought; 1854 Hydrology: Precipitation (3354); 3354 Meteorology and Atmospheric Dynamics: Precipitation (1854); 4522 Oceanography: Physical: El Nino. **Citation:** Lyon, B. (2004), The strength of El Niño and the spatial extent of tropical drought, *Geophys. Res. Lett.*, *31*, L21204, doi:10.1029/2004GL020901.

1. Introduction

[2] The intensity and duration of drought are two of the main driving forces behind their attendant impacts. Equally important, however, is the spatial extent of drought, an attribute that often receives comparatively less attention. In the tropics it is well established that drought frequently emerges as a rainfall response to El Niño, yet the areal extent of drought and its temporal variability has not been examined in detail, particularly among individual El Niño events and from a tropics-wide perspective. Related studies [*Dai et al.*, 1997, 1998; *Mason and Goddard*, 2001] have found an El Niño signal when examining the spatial coverage of anomalous aridity and wetness conditions on both regional and global scales. However, these studies did not look at the global tropics as a specific region, nor did they consider variability among individual El Niño events. Of course El Niño is not the only source of forcing for tropical drought. The protracted drought that gripped the Sahel during the 1970s and 1980s has recently been linked to long-term trends and variability of sea surface temperatures (SSTs) in the Indian and Atlantic oceans [*Giannini et al.*, 2004]. On seasonal to interannual timescales, SST forcing from outside the Pacific has also been associated with drought in eastern and southern Africa [*Goddard and Graham*, 1999] and northeastern Brazil [*Hastenrath*, 1984]. And regardless of its source, rainfall variability may be amplified by local land-atmosphere interactions [*Koster et al.*, 2000]. Nonetheless, from a global perspective and on interannual timescales El Niño (more generally, the El Niño - Southern Oscillation, or ENSO) remains the largest known source of rainfall variability in the tropics.

[3] Here an assessment of the temporal variation of the spatial extent of drought throughout the tropics was undertaken to address several fundamental questions arising from recent research. Are ENSO teleconnections stationary in time [*Nicholls et al.*, 1996; *Kumar et al.*, 1999; *Dai et al.*, 1998]? Is there evidence for a changing relationship between El Niño and the spatial extent of drought throughout the tropics? The observed upward trend in tropical SST in recent decades has been related to differing trend patterns in tropical precipitation over land and oceans in both observations and in models forced with observed tropical SST [*Kumar et al.*, 2004]. Is there a related trend in the extent of tropical drought? And given the multitude of mechanisms (and timescales) producing drought regionally, how dominant is the El Niño signal when examining drought from this tropics-wide scale?

2. Drought Definition and Spatial Extent Analysis

[4] Some answers to the above questions are provided through an analysis of a gridded, standardized precipitation index computed for all tropical land areas (within 30 deg. N-S of the equator). The index is based on gridded monthly precipitation analyses from the University of East Anglia (UEA) [*New et al.*, 2000] for the period 1950–1998 with supplementary data for 1999–2003 provided by the Climate Prediction Center's Merged Analysis of Precipitation (CMAP) [*Xie and Arkin*, 1996]. The index is computed at each gridpoint (0.5 × 0.5 deg. resolution for UEA data; 2.5 × 2.5 deg. for CMAP) and is based on 12-month overlapping sums of weighted, standardized monthly precipitation anomalies,

$$S_{12} = \sum_{i=1}^{12} \left(\frac{\log P_i - \overline{\log P_i}}{\sigma_i} \right) \cdot \frac{\overline{P_i}}{\overline{P_A}}. \quad (1)$$

In (1) P_i is the monthly precipitation of the ith month in the sum, overbars represent climatological averages, and σ_i represents the standard deviation of the anomalies of the log of monthly precipitation. P_A is the total annual precipitation and the weighting factor, P_i/P_A (representing the monthly fraction of annual precipitation), is used to dampen the large standardized anomalies resulting from small precipitation amounts near the start and end of dry seasons and to emphasize anomalies during the heart of rainy seasons. The sum, S_{12}, is then itself standardized to obtain a dimensionless measure of the relative severity of precipitation surplus

0094-8276/04/2004GL020901

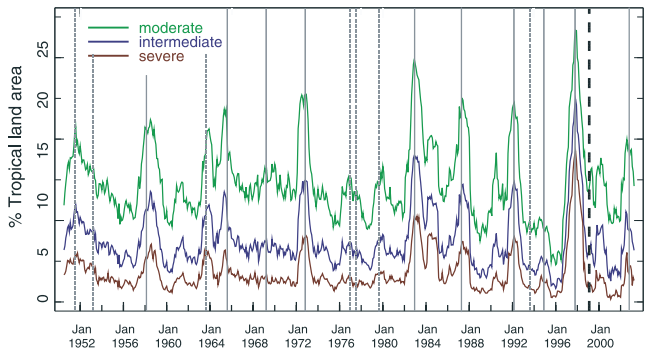

Figure 1. Time series (1951–2003) of the percent of tropical land area in drought for different levels of severity where green is moderate, blue intermediate, and red severe, based on the standardized 12-month precipitation index. The time series have been plotted with a 4-month lag relative to the solid vertical lines that indicate the time of maximum Nino 3.4 SST anomalies for the 10 strongest El Niño events. Dashed vertical lines are associated with the same but for the additional, weaker El Niño events identified in the analysis. Time series values to the right of the bold, dashed line are based on CMAP data.

or deficit over the proceeding 12 months. The index typically ranges from −2 (severe drought) to +2 (severe wetness) and is well correlated with other "drought" indices in the domain of interest such as the Palmer Drought Severity Index (PDSI). Desert regions, defined as having <96 mm of average annual precipitation, are masked from the analysis. This specific precipitation threshold was chosen in order to approximately match, visually, the dry masking to the major deserts in the domain, as identified elsewhere [*Hartmann*, 1994]. The overall results were not sensitive to the value of the precipitation threshold chosen. Using this index, time series of the percent of tropical land area in drought were generated, for different levels of severity [−1.0 (moderate), −1.5 (intermediate), −2.0 (severe)], for the period 1950 to 2003 as shown in Figure 1.

[5] In keeping with a priori expectations [*Dai et al.*, 1997, 1998], each of the major peaks in Figure 1, for all levels of drought severity, corresponds with the occurrence of El Niño. The typical sharpness of the peaks indicates the precipitation index is well suited for extracting the El Niño signal despite significant regional variability in the seasonality of both El Niño teleconnections [*Mason and Goddard*, 2001] and the annual cycle of precipitation. An important characteristic of drought seen in Figure 1 is its tendency to become more expansive during strong El Niño events (e.g., 1972–73, 1982–83, 1997–98). This characteristic has not been reported previously and cannot be captured, for example, in standard empirical orthogonal function (EOF) analysis, where a single spatial loading pattern of precipitation extremes (seasonal or annual) is associated with El Niño.

[6] The relationship between peak spatial extent of drought and El Niño was examined further. First, data from the extended reconstructed analysis of SST archived at the National Climatic Data Center [*Smith and Reynolds*, 2003] were used to compute SST anomalies averaged over the Nino 3.4 region of the tropical Pacific (5 deg. N-S, 120–170 deg. W). A 1961–1990 base period was used for computing SST anomalies and a 5-month running average was applied to the Nino 3.4 time series. An El Niño event was identified when the smoothed Nino 3.4 anomalies remained above 0.4 deg. C for at least 6 consecutive months. Figure 2 was constructed by plotting the maximum spatial extent of drought during El Niño events against the corresponding maximum SST anomaly for the Nino 3.4 region. There was typically about a 1 season (3–4 month) lag between the two maxima, Nino 3.4 leading.

[7] Figure 2 shows a remarkably robust, linear relationship between the two quantities for each category of drought ($r \cong 0.9$, $P < 0.001$ in Figure 2a). In addition, the spatial extent of drought for each category is seen to increase by roughly a factor of two between the weakest and strongest El Niño events. The standard definition of El Niño used here identifies 17 events in the study period, including three during the early to mid 1990s (as has been suggested elsewhere [*Goddard and Graham*, 1997]). When the weaker events are included in the analysis (Figure 2b) there is more scatter about the regression line. Nonetheless, the overall relationship is striking, especially when considering that some regional, teleconnected droughts fail to develop in a given El Niño, even during very strong events. In addition, both observations and model results [*Su and Neelin*, 2003] have indicated only a weak relationship between tropical averaged SST and precipitation (land and ocean) when

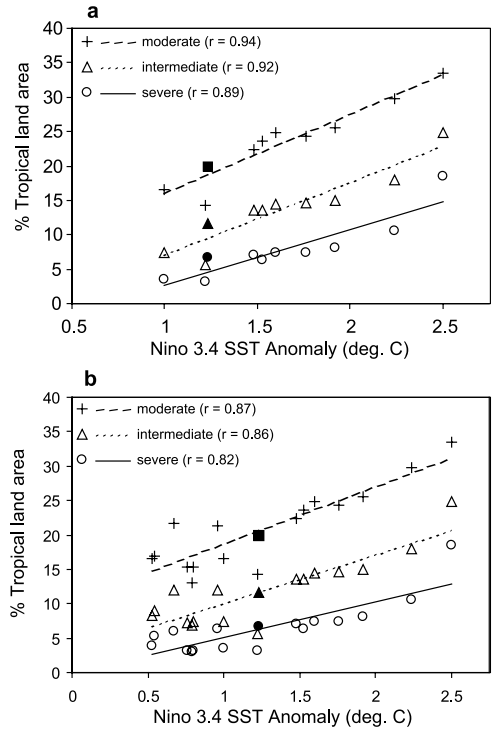

Figure 2. Scatter plots of peak drought extent (% of tropical land area, for three levels of drought severity) versus maximum Nino 3.4 SST anomaly (°C) during the associated El Niño with (a) showing the 10 strongest events and (b), all events from 1950–2003. The filled symbols are for the 2002–03 El Niño, where drought extent was computed using the CMAP data set.

seasonal (3-month) average anomalies are considered. This is clearly not the case when only considering land areas and drought.

3. Enhanced Likelihood of Drought

[8] An additional measure of the influence of El Niño on tropical drought was determined by first selecting those gridpoints where the occurrence of drought during El Niño was greater than that expected by chance ($p < 0.05$) for the period 1950–1998. For these gridpoints, the ratio of the number of months in drought during El Niño (28% of the time) to the number of months in drought at all other times (72%) was then computed for the period 1950 to 1998. In order to account for the observed tendency of maximum spatial extent of drought to lag maximum Nino 3.4 SST anomalies, a 4-month lag between these two time series was used when computing the ratio. This ratio is plotted in Figure 3 for the moderate and severe categories of drought (for emphasis, shading in the figure starts at ratio values >1). Figure 3a reveals the relative occurrence of moderate drought is enhanced during El Niño primarily in teleconnected regions, covering roughly 15% of the tropics (<7% area expected by chance). The relative occurrence of severe drought (Figure 3b) during El Niño is not only greater in much more of the tropics (34% of tropics; <2% expected by chance) than for the moderate category, but the ratio values increase significantly as well, reaching as high as 5 at several gridpoints. Taken together, the main findings of this study indicate that for a significant portion of the tropics severe drought is most likely to develop during an El Niño, and if it is a strong El Niño, drought is likely to cover a much greater extent of tropical land area.

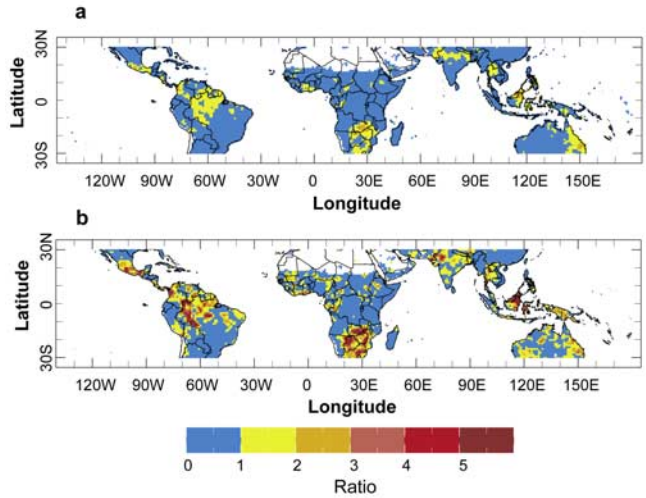

Figure 3. The ratio of the number of months a gridpoint was in drought during El Niño to the number of months in drought at all other times for different levels of severity. The top panel (a) is for moderate drought (standardized precipitation index values ≤ -1.0) and the bottom (b) for severe drought (precipitation index values ≤ -2.0). Ratio values >1 are plotted in shades of yellow to red.

4. Discussion

[9] From a mechanistic viewpoint, the use of Nino 3.4 SST anomalies to identify the existence and strength of El Niño is an arbitrary choice, insufficient to directly identify the physical cause(s) that link El Niño to drought extent. Diagnostic modeling studies, for example, indicate that tropical precipitation deficits associated with El Niño likely result from regionally varying mechanisms [*Su and Neelin*, 2002]. However, in response to the anomalous heating in the eastern tropical Pacific following the onset of El Niño the tropically averaged tropospheric temperature typically increases (along with tropically averaged SST) [*Sobel et al.*, 2002]. Recent theoretical work supported by modeling studies [*Chiang and Sobel*, 2002; *Neelin et al.*, 2003] suggests that the stabilizing effect such an anomalously warm troposphere has on convection initiates the tropical teleconnected precipitation response during El Niño, which is then modified regionally depending on the character of the underlying surface, land-atmosphere interaction, and varying aspects of the atmospheric circulation. A connection between Nino 3.4 SST and a tropics wide forcing mechanism therefore does appear to exist.

[10] Here the maximum tropical tropospheric temperature anomalies accompanying El Niño were computed based on the NCEP-NCAR Reanalysis (averaged from 850–200 hPa, within 30 deg. N-S of the equator; base period 1980–2003) [*Kistler et al.*, 2001] and correlated with associated peak drought extent. The correlation for the five events occurring after 1980, when the data is most reliable, was near or exceeded 0.9, although only a single maxima in tropospheric temperature was observed during the first half of the 1990s. Given the correlation between Nino 3.4 SST anomalies and those in the tropical troposphere, this correlation clearly does not provide conclusive evidence of a forcing mechanism. The result is nonetheless an interesting finding.

[11] What are the implications for El Niño related droughts of the future? There is observational evidence [*Trenberth and Hurrell*, 1999], though controversial in terms of its underlying cause [*Wunsch*, 1999; *Federov and Philander*, 2000], of an increase in the frequency and strength of El Niño events in recent decades. Whether this is related to greenhouse warming is debatable [e.g., *Kumar et al.*, 1999], nonetheless the current results indicate a consequence of stronger and more frequent El Niños will be more expansive drought, and increased frequency of severe drought, in the tropics. The extent to which the El Niño and drought extent relationship may serve as a proxy for future tropical climate variations expected under global warming is not clear, though some similarities are likely [*Neelin et al.*, 2003]. In any case, increasing air temperatures will exacerbate tropical droughts, regardless of whether or not they play a role in helping to produce them.

[12] **Acknowledgments.** The author thanks A. Barnston, M. Cane, A. Sobel, A. Giannini and C. Ropelewski for their insights, comments, and careful reading of the original manuscript. IRI is supported by the NOAA Office of Global Programs and Columbia University.

References

Chiang, J. C. H., and A. Sobel (2002), Tropical tropospheric temperature variations caused by ENSO and their influence on the remote tropical climate, *J. Clim.*, *15*, 2616–2631.

Dai, A., I. Y. Fung, and A. D. Del Genio (1997), Surface observed global land precipitation variations during 1900–88, *J. Clim.*, *10*, 2493–2962.

Dai, A., K. E. Trenberth, and T. R. Karl (1998), Global variations in droughts and wet spells: 1900–1995, *Geophys. Res. Lett.*, *25*, 3367–3370.

Federov, A. V., and S. G. Philander (2000), Is El Niño changing?, *Science*, *288*, 1997–2002.

Giannini, A., R. Saravanan, and P. Chang (2004), Oceanic forcing of Sahel rainfall on interannual to interdecadal time scales, *Science*, *302*, 1027–1030.

Goddard, L., and N. E. Graham (1997), El Niño in the 1990s, *J. Geophys. Res.*, *102*, 10,423–10,436.

Goddard, L., and N. E. Graham (1999), Importance of the Indian Ocean for simulating rainfall anomalies over eastern and southern Africa, *J. Geophys. Res.*, *104*, 19,099–19,116.

Hartmann, D. L. (1994), *Global Physical Climatology*, 411 pp., Academic, San Diego, Calif.

Hastenrath, S. (1984), Predictability of northeast Brazil drought, *Nature*, *307*, 531–533.

Kistler, R., et al. (2001), The NCEP-NCAR 50-year Reanalysis: Monthly means CD-ROM and documentation, *Bull. Am. Meteorol. Soc.*, *82*, 247–268.

Koster, R. D., M. J. Suarez, and M. Heiser (2000), Variance and predictability of precipitation at seasonal-to-interannual timescales, *J. Hydrometeorol.*, *1*, 26–46.

Kumar, K. K., B. Rajagopalan, and M. A. Cane (1999), On the weakening relationship between the Indian Monsoon and ENSO, *Science*, *284*, 2156–2159.

Kumar, A., F. Yang, L. Goddard, and S. Schubert (2004), Differing trends in the tropical surface temperatures and precipitation over land and oceans, *J. Clim.*, *17*, 653–664.

Mason, S. J., and L. Goddard (2001), Probabilistic precipitation anomalies associated with ENSO, *Bull. Am. Meteorol. Soc.*, *82*, 619–638.

Neelin, J. D., C. Chou, and H. Su (2003), Tropical drought regions in global warming and El Niño teleconnections, *Geophys. Res. Lett.*, *30*(24), 2275, doi:10.1029/2003GL018625.

New, M., M. Hulme, and P. Jones (2000), Representing twentieth century space-time climate variability. Part II: Development of 1901–96 monthly grids of terrestrial surface climate, *J. Clim.*, *13*, 2217–2238.

Nicholls, N., B. Lavery, C. Frederiksen, and W. Drosdowsky (1996), Recent apparent changes in relationships between the El Niño–Southern Oscillation and Australian rainfall and temperature, *Geophys. Res. Lett.*, *23*, 3357–3360.

Smith, T. M., and R. W. Reynolds (2003), Extended reconstruction of global sea surface temperatures based on COADS data (1854–1997), *J. Clim.*, *16*, 1495–1510.

Sobel, A. H., I. M. Held, and C. S. Bretherton (2002), The ENSO signal in tropical tropospheric temperature, *J. Clim.*, *15*, 2702–2706.

Su, H., and J. D. Neelin (2002), Teleconnection mechanisms for tropical Pacific descent anomalies during El Niño, *J. Atmos. Sci.*, *59*, 2694–2712.

Su, H., and J. D. Neelin (2003), The scatter in tropical average precipitation anomalies, *J. Clim.*, *16*, 3966–3977.

Trenberth, K. E., and J. E. Hurrell (1999), Comments on: The interpretation of short climate records, with comments on the North Atlantic and Southern Oscillations, *Bull. Am. Meteorol. Soc.*, *80*, 2721–2722.

Wunsch, C. (1999), The interpretation of short climate records, with comments on the North Atlantic and Southern Oscillations, *Bull. Am. Meteorol. Soc.*, *80*, 245–255.

Xie, P., and P. A. Arkin (1996), Analysis of global monthly precipitation using gauge observations, satellite estimates and numerical model predictions, *J. Clim.*, *9*, 840–858.

B. Lyon, International Research Institute for Climate Prediction, Lamont-Doherty Earth Observatory, Columbia University, New York, NY 10964, USA. (blyon@iri.columbia.edu)